J Mol Model (2013) 19:1995–2005
DOI 10.1007/s00894-012-1583-0

ORIGINAL PAPER

Structural, mechanical and electronic properties of *nano-fibriform* silica and its organic functionalization by dimethyl silane: a SCC-DFTB approach

Maurício Chagas da Silva · Egon Campos dos Santos · Maicon Pierre Lourenço · Hélio Anderson Duarte

Received: 31 May 2012 / Accepted: 23 August 2012 / Published online: 18 September 2012

Abstract Self-consistent-charge density-functional tight-binding (SCC-DFTB) approximated method was employed to investigate the structural, mechanical and electronic properties of the zigzag and armchair *nano-fibriform* silica (SNTs) and their outer surface organic modified derivatives (MSNTs) with internal radii in the range of 8 to 36 Å. The strain energy curves showed that the nanotubes structures are energetically more stable compared to the respective sheet structures. External hydroxyl dihedral angles in silica nanotubes have small influence, about 0.5 meV.atom^{-1}, in the strain energy curve tendency of those materials favoring the zigzag chirality. The chemical modification of outer surface of SNTs by dimethyl silane group affects their relative stability favoring the armchair chirality in approximately 2 meV.atom^{-1}. MSNTs have axial elastic constants, Young's moduli, determined at the harmonic approximation, around 100 GPa smaller than the respective SNTs. The Young's moduli of zigzag and armchair SNTs are in the range of 150–195 GPa and 232–260 GPa, respectively. And for the zigzag and armchair MSNTs these values are in the range of 77–89 and 110–140 GPa, respectively. The SNTs and MSNTs were characterized as insulators with band gaps around 8–10 eV.

Keywords Nano-fibriform · Organic functionalization · SCC-DFTB · Silica · Tight-binding

Electronic supplementary material The online version of this article (doi:10.1007/s00894-012-1583-0) contains supplementary material, which is available to authorized users.

M. C. da Silva · E. C. dos Santos · M. P. Lourenço · H. A. Duarte (✉)
Grupo de Pesquisa em Química Inorgânica Teórica, Departamento de Química, ICEx – Universidade Federal de Minas Gerais, 31270-901, Belo Horizonte, MG, Brazil
e-mail: duarteh@ufmg.br

Introduction

Since the discovery of carbon nanotubes (CNTs) [1], new nanostructured materials have been synthesized by different research groups and applied by industries to develop new technological devices. CNTs have received great attention from the scientific community furthermore inorganic nanotubes have also been the subject of many studies. Inorganic nanotubes such as WS_2 [2], BN, BC_2N [3, 4], GaS [5], MoS_2 [6], imogolite (Al_2O_3-$SiOH(OH)_3$) [7–9] and silica nanotubes (SNT – $(SiO_2)_x(OH)_y$) have been extensively studied. However, most of these inorganic nanotubes are difficult to synthesize or to obtain from the nature excepted nanostructured clay minerals. The increasing interest for these silica based nanostructured materials is due to their physical and chemical stability and the facility to modify them through chemical functionalization. Therefore, it is important to study the electronic, mechanical and structural aspects related to silica nanostructured compounds, aiming to contribute to the development of new advanced materials.

The most common structure of silica is α-quartz with the tetrahedron SiO_4 as a main structural unit. Due to the large range of SiOSi angles there are some different crystal phases such as β-cristobalite and silica rods, clusters, rings, chains, nanowires and nanotubes as well [10, 11]. Considering the one-dimensional silica nanomaterial, silica nanowires have been employed in high strength light source as light-emitting diodes. Amorphous SiO_2 nanowire was synthesized in exciter laser ablation method by Yu et al. [12] . In some other synthetic pathways a mild sol–gel process is used to develope nanotubular silica as well. An example of a simple synthetic pathway was used by Wang et al. [13, 14] to produce silica nanotube in a process that removes the brucite layer by acid leaching of chrysotile. Wang et al. [15]

also modified the external surface of silica nanotubes using $SiCl_2(CH_3)_2$ to produce outer surface modified silica nanotubes (MSNTs) with dimethyl silane groups.

Recently, SNTs have been applied to biological and environmental systems because of their specificities and large surface area. Kim et al. [16] developed silica nanotubes materials as microcapsule to delivery drugs. Polymer-based drug delivery systems have limitation because of hydrolysis and erosion of these materials as pointed out by Kim et al. [16]. Bai et al. [17] synthesized a mesoporous silica nanotubes via a sol–gel process to immobilize a lipase enzyme. A range of enzymes like penicillin G acylase, glucose oxidase, α-amylase, Mucor Javaniscus lipase, glucose isomerase and others have been immobilized on mesoporous silicate nanotubes as reported by Bai et al. [17]. These possibilities allow the development of a new class of biological heterogeneous catalysts.

For a long time, silica compounds have been employed as support for different catalysts in industries. Structured silicate materials like clay minerals and zeolites can be cited as support (adsorbent) and also in some cases as a true catalyst. As catalyst supports, SNTs have many advantages such as acid and base chemical attack resistance, they are not thermolabel materials, and they also present different molecular structures with a wide range of size and shape of porous. Qiang et al. [18] employed SNTs as support of cobalt catalyst for Fischer-Tropsch synthesis. High effects of the SNTs structures to physicochemical and catalytic properties of cobalt-based catalysis in Fischer-Tropsch synthesis are reported by Qiang et al. [18] and concluded that Co/SNTs have higher catalytic activity than Co/CNT.

Due to the huge SNTs potential applications in chemical reactions and in the development of new materials, we decided to investigate the stability and the electronic, mechanical and structural properties of SNTs and MSNTs using the SCC-DFTB method which has been used with remarkable success to investigate similar systems [19].

Computational details

Silica *nano-fibriform* (SNT) and modified silica nanotubes (MSNT) by dimethyl silane functionalization were investigated starting from the respective idealized sheet structures. Based on the elemental analysis reported by Wang et al. [13, 15], primitive unit cells representing the silica and the modified silica nanotubes were built, some of which are presented in Fig. 1. Figure 2 shows the sheets that originate the SNTs and MSNTs and the chiral vector for armchair and zigzag absolute configurations used to generate the nanotubes in the present work. Different sizes and chiralities of silica *nano-fibriform* were built with inner radius variation in a range of 8 to 36 Å.

The self-consistent-charge density-functional tight-binding approximation (SCC-DFTB) [20, 21] was used to study all periodic systems. The DFTB+ package [22, 23] was employed with the parameters (Slater-Koster tables) developed by Seifert and collaborators [24–27] to optimize all structures and to do post-process calculations. For the silica sheet systems, Fig. 2, the periodicity was set in x and y axis, and in the z direction a vacuum was simulated, setting the respective cell parameter in z direction around 100 Å. Therefore, an orthorhombic cell was used for the silica sheet systems ($a \neq b \neq c$ and $\alpha=\beta=\gamma=90^{o}$). The periodicity of the nanotubes presented in Fig. 3 and 4 was set in the y direction while in the x and z directions a vacuum was simulated as described for the silica sheet systems. For the nanotubes a tetragonal cell was set ($a=c \neq b$ and $\alpha=\beta=\gamma=90^{o}$).

All atoms in the unit cells were optimized with no constraint using a conjugated-gradient algorithm implemented in

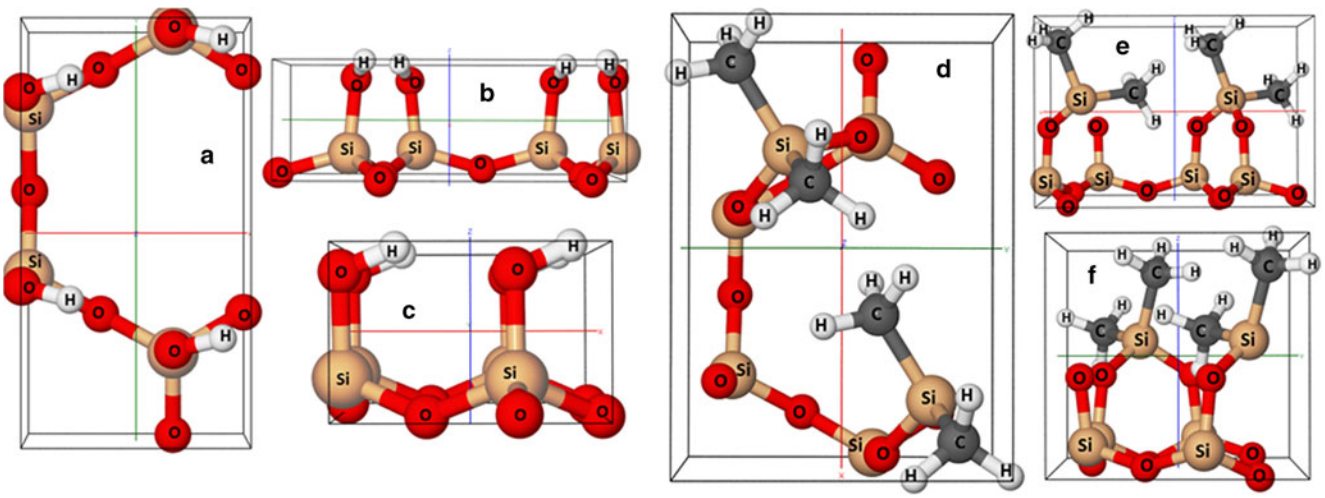

Fig. 1 Top (**a**) and side (**b,c**) views of the unit cell of the sheet used to generate the silica nanotubes; top (**d**) and side (**e,f**) views of the unit cell of the sheet used to generate the modified silica nanotubes

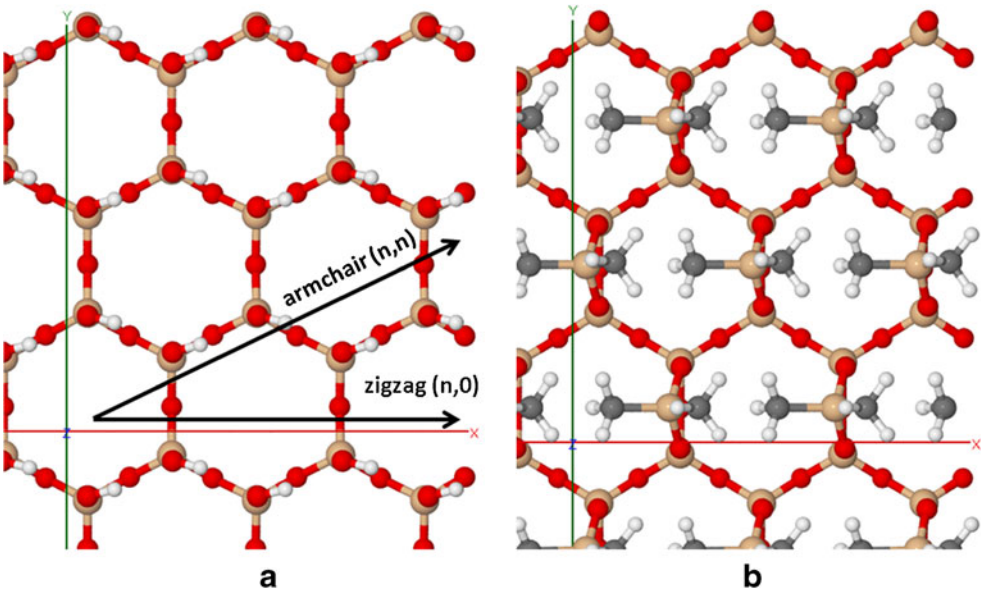

Fig. 2 (**a**) Silica sheet with the chirality vector representation and (**b**) the modified one

DFTB+ package. The cell parameters, *a* and *b* for the silica sheets and *b* for SNTs and MSNTs, were optimized by simplex algorithm [28–30] adapted to DFTB+ package by the authors. See supporting information for the Fortran code of this simplex implementation. In each simplex step all atoms presented in the unit cell were fully optimized. A Monkhorst-Pack [31] sampling was used to generate a converged 2×4×1 k-points for silica sheet systems and 1x4x1 for SNT and MSNT systems that were used in all calculations.

Results and discussion

The values of the inner radius (R_{in}) and the optimized unit cell parameters (ε) for the SNT and MSNT in the equilibrium geometries are presented in Tables 1 and 2. The inner radius (R_{in}) was defined with the mean value of all oxygen atom positions inside the SNT and MSNT. The zigzag chirality has much larger values of unit cell parameters compared to armchair chirality for both SNT and MSNT. For the zigzag chirality the unit cell parameter is around 9.0 Å and for the armchair it is around 5.3 Å. However, comparing the inner radii of the nanotubes in Tables 1 and 2 for the same number of repetition units (n), the zigzag SNT and MSNT are smaller than the respective armchair SNT and MSNT. The modification of the outer surface by dimethyl silane groups decreased the unit cell parameter in 0.1 Å in armchair chirality, approximately. However, an opposite effect is observed for zigzag chirality, the unit cell parameter increased in 0.1 Å with the outer surface modification. The inner radii increased with the functionalization for both chiralities.

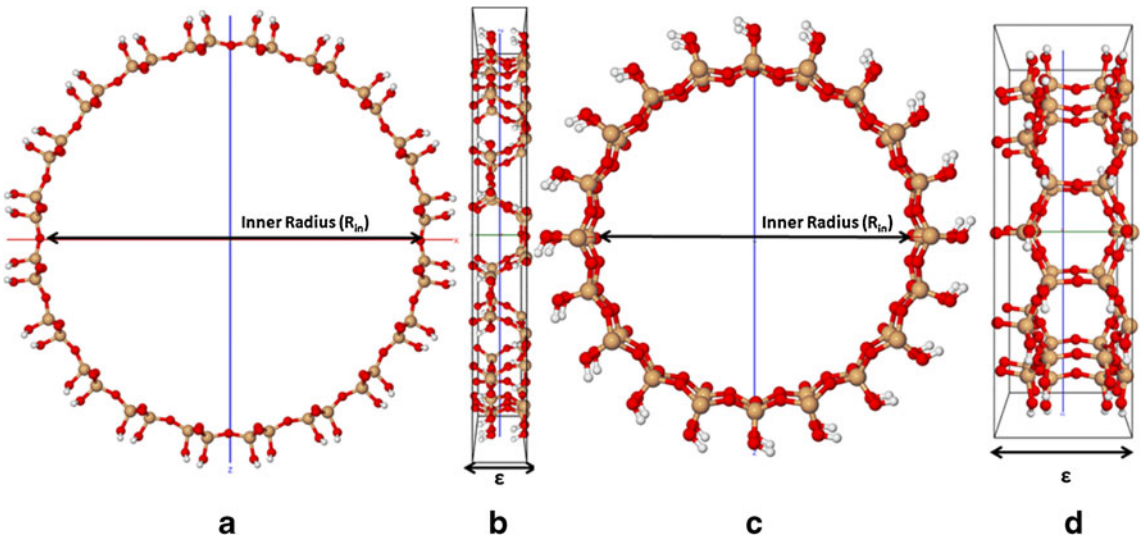

Fig. 3 (**a**) *Axial* and (**b**) *side views* of (n,n) armchair SNT; (**c**) *axial* and (**d**) *side views* of (n,0) *zigzag* SNT. ε is the unit cell parameter of the nanotube

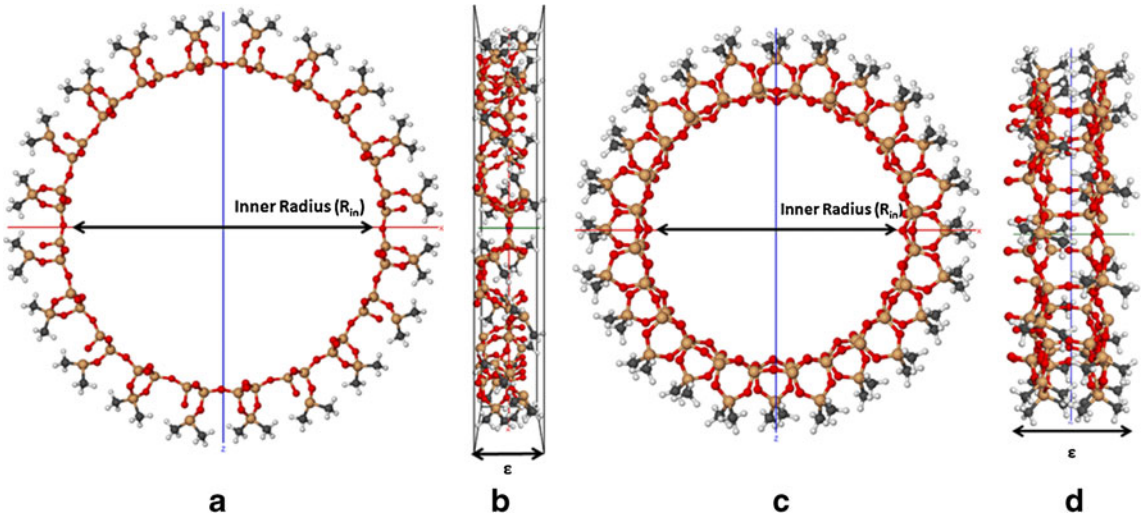

Fig. 4 (**a**) *Axial* and (**b**) *side views* of (n,n) armchair MSNT; (**c**) *axial* and (**d**) *side views* of (n,0) *zigzag* MSNT. ε is the unit cell parameter of the nanotube

In Table 3 some structural parameters of the SNTs and MSNTs are presented. The values of SiO bond distances and OSiO and SiOSi angles are in good agreement to those values reported by Ju et al. [10] and Nicholas et al. [32] based on the XRD of zeolites and crystalline silica and on molecular mechanics and *ab initio* calculations of silica compounds, respectively. Table 3 indicates that Si is in a tetrahedral or slightly distorted structural arrangement. We did not observe large effects due to chirality or outer surface modification. However, a larger influence was observed for SiOSi angles which were around 3° larger for zigzag SNT compared to the armchair SNTs and at least 5° smaller for the MSNTs compared to the respective SNTs. These variations are reported by Ju et al. [10] as an associated effect of the accentuated anharmonicity with small force constants for bending deformation of those angles.

The strain energy (E_s) is defined by Eq. 1 where E_{NT} is the energy per atom of the nanotube and E_p is the energy per atom of the respective sheet structure. The tendency of strain energy of SNTs and MSNTs are presented in Fig. 5.

$$E_s = E_{NT} - E_p \tag{1}$$

The strain energy can be interpreted as the energy necessary to roll the sheet and build the nanotube. The strain energy curves, Fig. 5, indicate clearly that SNTs and MSNTs are more energetically favorable compared to the sheets. This tendency is similar to the one presented by Seifert et al. [33] for armchair and zigzag SiH nanotubes. The behavior of the strain energy curve is completely different for the inorganic [6] and clay mineral nanotubes [7] which is positive asymptotically reaching the sheet energy for larger radii. The imogolite and germanium-like imogolite nanotubes are the only exception, which present a minimum in the strain energy curve and the asymptote for larger radii reaches the sheet energy value (E_{strain}=0) from the negative values. However, for the SiH nanotube calculated by Seifert et al. [30] and the present SNTs and MSNTs the strain energy curves have an unusual behavior.

Table 1 Optimized cell parameters (ε), inner radius (R_{in}), number of atoms in the nanotube unit cell (N_a) and energy per atom (E_a) obtained for the armchair and zigzag SNTs

N_a	n	Armchair (n,n)			Zigzag (n,0)		
		ε (Å)	R_{in} (Å)	E_a (h/atom)	ε (Å)	R_{in} (Å)	E_a (h/atom)
180	10	5.382	14.1	−2.305522	9.052	8.7	−2.305751
216	12	5.385	17.0	−2.305501	9.068	10.0	−2.305703
252	14	5.387	19.9	−2.305484	9.079	11.8	−2.305662
288	16	5.394	22.8	−2.305470	9.087	13.5	−2.305629
324	18	5.393	25.7	−2.305458	9.094	15.3	−2.305603
360	20	5.394	28.6	−2.305449	9.099	17.0	−2.305580
396	22	5.391	31.6	−2.305440	9.098	18.7	−2.305561
432	24	5.393	34.5	−2.305433	9.106	20.4	−2.305546

Table 2 Optimized cell parameters (ε), inner radius (R_{in}), number of atoms in the nanotube unit cell (N_a) and energy per atom (E_a) obtained for the armchair and zigzag MSNTs

N_a	n	Armchair (n,n)			Zigzag (n,0)		
		ε (Å)	R_{in} (Å)	E_a (h/atom)	ε (Å)	R_{in} (Å)	E_a (h/atom)
320	10	5.324	14.8	−1.693108	9.150	8.6	−1.693049
384	12	5.257	17.9	−1.693098	9.121	10.4	−1.693012
448	14	5.236	20.9	−1.693025	9.133	12.1	−1.692959
512	16	5.282	23.9	−1.692966	9.146	13.8	−1.692943
576	18	5.313	26.7	−1.692912	9.144	15.6	−1.692913
640	20	5.317	29.7	−1.692891	9.181	17.2	−1.692889
704	22	5.311	32.7	−1.692872	9.169	19.0	−1.692868
768	24	5.321	35.6	−1.692857	9.204	20.6	−1.692851

The strain energy becomes more negative for smaller radii as presented in Fig. 5. Indeed, this is expected since the silica nano-fibriform is obtained from the mild acid leaching of the chrysotile removing the brucite ($Mg(OH)_2$) outer layer and leaving the silica fibriform intact. Therefore, the SNTs are local minima in the potential energy surface, decreasing the radii the system will eventually collapse to the amorphous silica. However, as indicated by the experiments realized by Wang et al. [13, 14], after the acid leaching of the chrysotile, the silica remains with *nano-fibriform* structure. The SNTs and MSNTs are mechanically reasonably stable as we discuss below.

For the MSNTs, it is clear that the chirality affects the stability of the system. The zigzag MSNTs is, at least, 2.2 meV.atom^{-1} less stable than the armchair structure. In zigzag MSNT, methyl groups are closer to each other, increasing steric hindrance, which could consequently increase the electronic energy, as shown in Fig. 6. In the armchair MSNTs, methyl groups are more disperse decreasing the steric hindrance. A small differentiation between armchair and zigzag strain curves was also observed to SNTs. It can be seen for SNT strain energy curve in Fig. 5, that zigzag chirality is 0.5 meV.atom^{-1} more stable than armchair chirality. Zigzag SNT's superficial hydroxyl groups are orientated to maximize hydrogen bond between hydroxyl neighbor groups as shown in the Fig. 7. However, armchair SNT's superficial hydroxyl groups are not oriented to maximize hydrogen bond between hydroxyl neighbor groups as presented at Fig. 7. Hence, these facts explain the small stabilization of zigzag chirality compared to armchair for SNTs.

Potential energy curves near the minimum were built during simplex unit cells optimization processes to all nanotubes. Flat shape curves were observed for SNTs compared to MSNTs. Polynomials were fit to this potential curve to find out approximated values of axial elastic constants to the nanotubes. Considering the literature [34–36], the polynomials coefficients can be related to elastic constants of the materials. In a harmonic approximation, the second coefficients in Taylor's expansions of energy is related to Young's modulus (Y) by Eq. 2, as discussed in detail by Lier et al. [36], Oh [35] and Marana et al. [34]. In Eq. 2, ε is the dimensionless elongation of the nanotube in axial orientation, V is the volume of the unit cell and σ is the stress function applied to deform the system away from its minimum.

$$Y = \frac{1}{V}\left(\frac{d^2\sigma(\varepsilon)}{d\varepsilon^2}\right)_{\varepsilon=0} \tag{2}$$

Young's moduli (Y) estimates for SNTs and MSNTs are presented in Tables 4 and 5. The armchair SNTs present larger Young's moduli than the respective zigzag ones by about 150 GPa. Young's moduli of the armchair MSNTs are larger than the zigzag ones in about 40 GPa. The modification of the SNTs with dimethyl silanes leads to the decrease of Young's Moduli of about 100 GPa for both chiralities. As

Table 3 Mean values and deviations for SiO and SiC bond distances and OSiO and SiOSi angles of SNT and MSNT

Structural parameter	Armchair		Zigzag	
	SNT	MSNT	SNT	MSNT
SiC (Å)	–	1.885±0.002	–	1.8833±0.0005
SiO (Å)	1.642±0.0004	1.640±0.001	1.639±0.001	1.640±0.001
OSiO (º)	109.36±0.04	109.33±0.01	109.41±0.01	109.19±0.01
SiOSi (º)	145.0±0.8	140±1	148±2	140±2

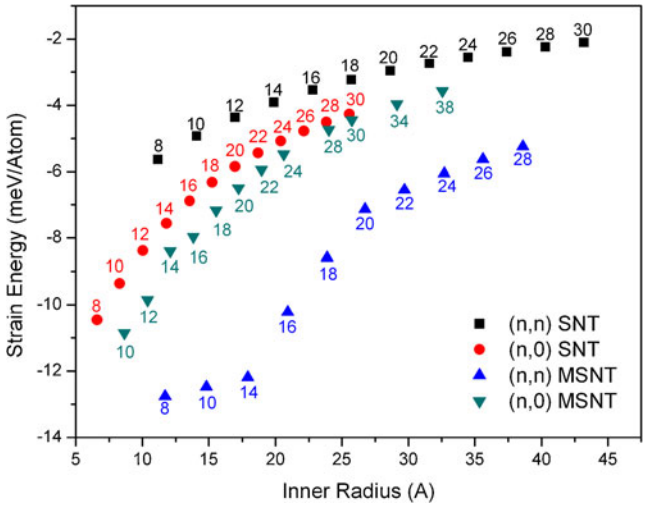

Fig. 5 SNT and MSNT strain energy curves with respect to the inner radius for armchair and zigzag chiralities

discussed before, this decrease is probably due to the σ electronic inductive effects of methyl groups that enhance the electronic density of the materials and consequently decrease the force of chemical bonds.

Seifert et al. [33] reported Young's Moduli around 50–80 GPa to SiH nanotubes and Guimarães et al. [7, 37] reported values for imogolite and halloysite around 400–300 and 230–320 GPa, respectively. The Young's moduli of SNTs and MSNTs are larger than those reported for SiH, but smaller than those reported for nanostructured clay minerals using the same level of theory. Recently, Lourenço et al. [19] reported the SCC-DFTB calculations of the single walled chrysotile nanotubes. The Young moduli of the zigzag and armchair chrysotile nanotubes are calculated to be in a range of 261–320 GPa. Comparing these values to the SNTs, it is clear that the brucite, $Mg(OH)_2$, layer in the outer part of the chrysotile, increases the stiffness of the nanotube structure. The Young's moduli of the zigzag SNTs is about 40 GPa smaller than of the zigzag chrysotile nanotubes. For the armchair, this difference is about 100 GPa. The presence of the brucite layer in the chrysotile provides greater mechanical stability.

It can be seen by the linear correlation coefficients (R^2) and by square summation model deviations ($\chi 2$) presented in Tables 4 and 5 that the harmonic approximation of potential energy curve for SNTs and MSNTs was adequate. However, in some cases larger deviations were observed, as for (12,12) and (14,14) armchair SNTs. For (12,12) and (14,14) SNTs, poorer values of R^2 and $\chi 2$ were obtained, 0.97 and 8.10^{-15} respectively, if compared to the other SNTs. Only in these cases the harmonic approximation has some limitation for describing the potential energy curve. As a consequence, the errors associated with the determinations of Y are also larger for these chiralities, around ±10 GPa. In the other cases, the errors are around ±1 GPa as presented in Tables 4 and 5. The harmonic approximation was better fit to

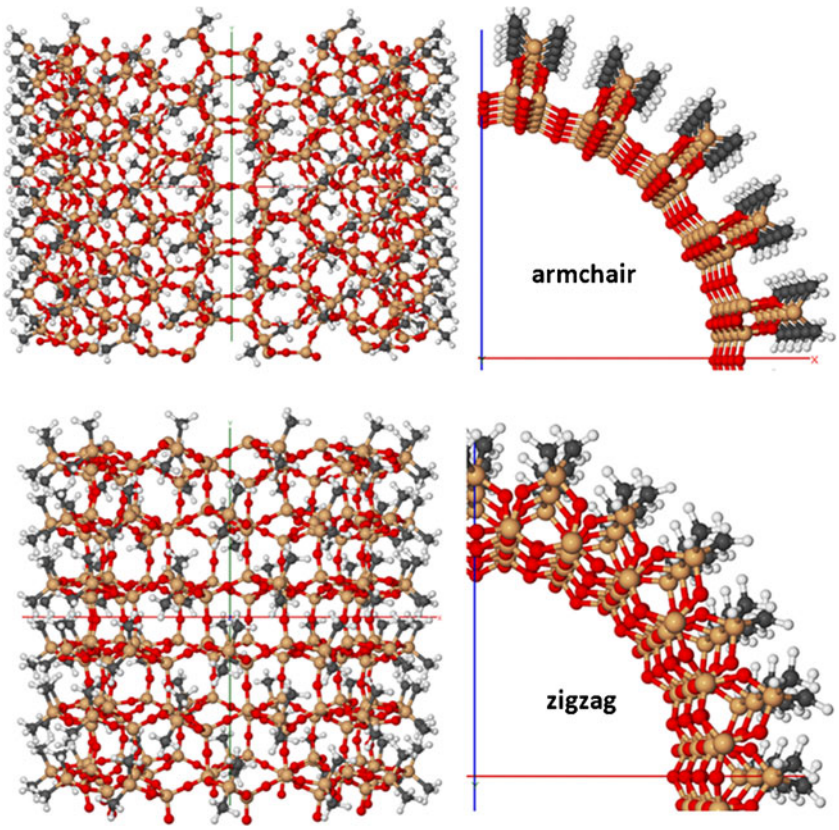

Fig. 6 Dimethyl silane orientation in the MSNTs

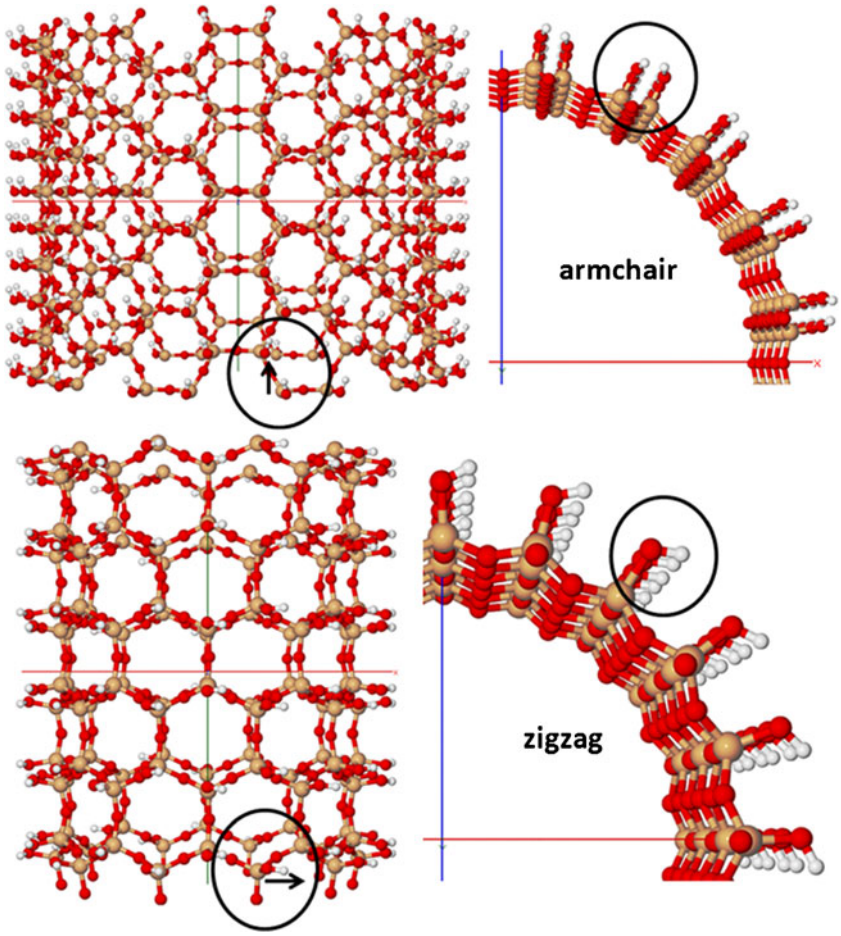

Fig. 7 Hydroxyl group orientation in the SNTs

MSNTs than to SNTs because of the small observed values for $\chi 2$ in MSNT presented in Table 5.

The electronic band structures were calculated in the first Brillouin zone and the electronic band gap transitions were estimated for SNTs and MSNTs. The electronic band structures following the path *Γ-X-M-Γ-Z-R-A-Γ* in the first Brillouin zone were calculated to SNTs and MSNTs. A sample of representative electronic band structures to SNTs and MSNTs are presented in Fig. 8. A direct electronic band gap was observed for SNTs and occurred over the *Γ* point. A direct electronic band gap was also observed for armchair MSNTs but over the *X* point, but an indirect band gap was calculated for zigzag MSNTs. The indirect electronic band gap observed to zigzag MSNTs occurred between *X* and *Γ* points.

SNTs and MSNTs are insulator materials with band gaps around 9.8 eV and 8.5 eV, respectively. The band gap calculated for SNTs and MSNTs are presented in Table 6. The chirality did not affect the band gap values, but the outer surface functionalization modified in 1 eV the band gaps, as shown in Table 6. Dimethyl silane groups change the

Table 4 Young's modulus (Y), linear correlation coefficient (R^2) and square summation model deviation (χ^2) in polynomial adjust of degree 2 of potential curve of SNT in armchair and zigzag chiralities

n	Armchair (n,n)			Zigzag (n,0)		
	Y(GPa)	R^2	χ^2 (10^{-15}) [a]	Y(GPa)	R^2	χ^2 (10^{-15})[a]
10	232±2	0.9992	0.30	145±1	0.9998	3.05
12	231±7	0.9743	8.00	156±1	0.9998	1.92
14	225±9	0.9698	4.00	165±1	0.9998	1.00
16	347±2	0.9998	0.07	173±1	0.9998	0.80
18	350±3	0.9994	0.03	184±1	0.9999	0.37
20	357±1	0.9999	0.01	183±1	0.9996	1.29
22	360±1	0.9999	0.06	187±3	0.9986	3.22
24	359±1	0.9999	0.02	194±2	0.9993	1.23

[a] $\chi^2 = \sum_{i=1}^{M} (y_i - \hat{y}_i)^2$: M is the numbers data; y_i is the calculated energy; and $\hat{y}_i$ is the adjusted energy by the polynomial model

Table 5 Young's modulus (Y), linear correlation coefficient (R^2) and square summation model deviation (χ^2) in polynomial adjust of degree 2 of potential curve of SNT in armchair and zigzag chiralities

n	Armchair (n,n)			Zigzag (n,0)		
	Y(GPa)	R^2	χ^2 $(10^{-16})^a$	Y(GPa)	R^2	χ^2 $(10^{-16})^a$
10	116.5±0.6	0.9999	0.96	89±2	0.9991	0.79
12	139.9±0.3	0.9999	0.55	88±1	0.9994	0.56
14	132.0±0.6	0.9999	0.24	80,5±0.4	0.9999	0.07
16	126.8±0.2	0.9999	0.02	82.2±0.8	0.9996	0.23
18	112.6±0.5	0.9998	0.61	77±2	0.9986	0.85
20	111.9±0.9	0.9998	1.20	76±1	0.9997	0.20
22	110±1	0.9992	2.09	79±2	0.9995	0.37
24	111.9±0.7	0.9999	0.81	83±1	0.9991	0.63

[a] $\chi^2 = \sum_{i=1}^{M} (y_i - \hat{y}_i)^2$: M is the numbers data; y_i is the calculated energy; and $\hat{y}_i$ is the adjusted energy by the polynomial model

electrical properties of SNTs, decreasing the band gaps. This effect can be explained again by σ electronic inductive effects due to the presence of dimethyl silane groups on the outer surface. The net electronic charge distribution over the SNTs and MSNTs is shown in Fig. 9. The presence of the dimethyl silanes leads the outer surface of the MSNTs to be almost neutral, indicating that the surface became more hydrophobic as expected.

Conclusions

Silica *nano-fibriform* and their outer functionalized surface derivatives have been investigated by SCC-DFTB method. The silica *nano-fibriform* obtained from mild acid leaching of chrysotile in which the brucite ($Mg(OH)_2$) layer is removed and the external surface is functionalized with dimethyl silane groups have been recently reported [15]. The

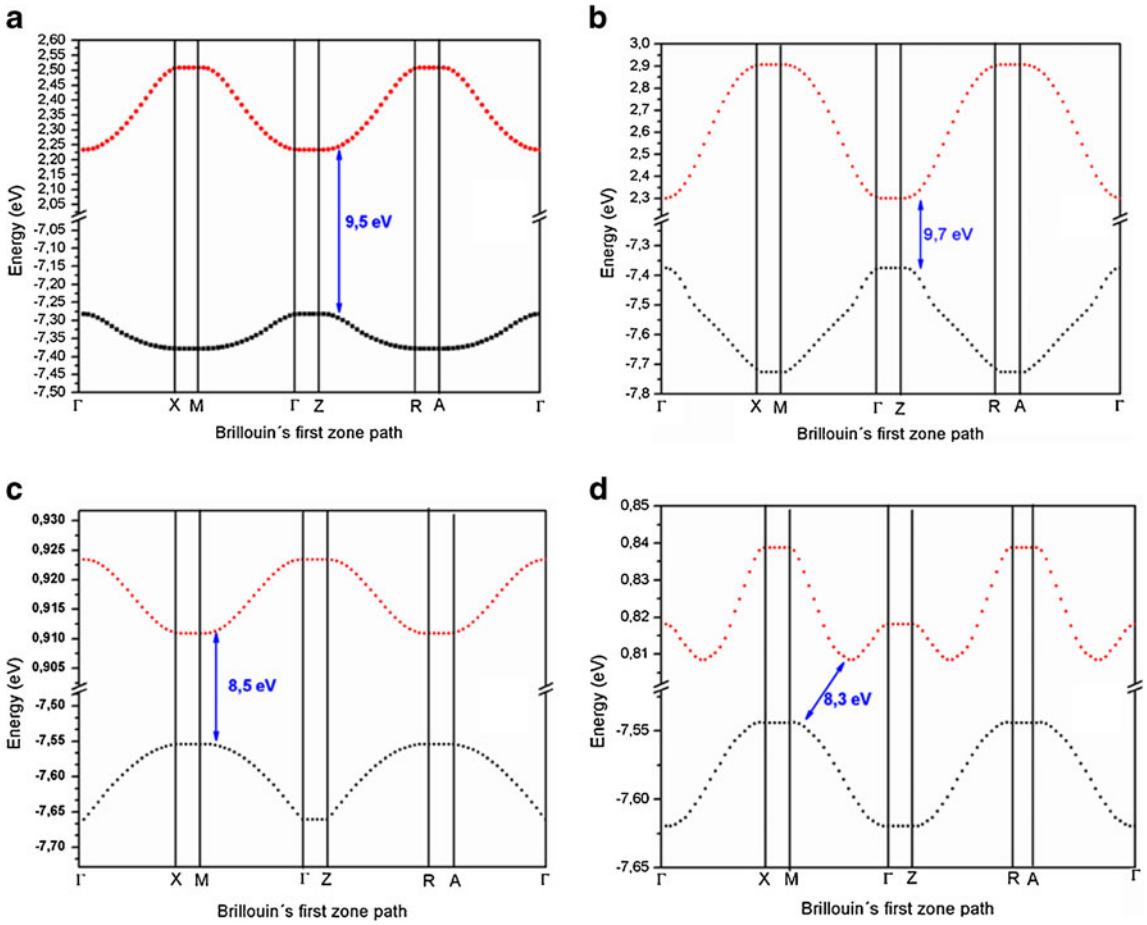

Fig. 8 Electronic band structure of (**a**) armchair SNTs, (**b**) *zigzag* SNTs, (**c**) armchair MSNTs and (**d**) *zigzag* MSNTs. Color of lines: *red*, conduction band; *black*, valence band

Table 6 Calculated band gaps to SNT and MSNT as a variation of number of unit cell repetition (n). Values expressed in eV

n	SNTs		MSNTs	
	(n,0)	(n,n)	(n,0)	(n,n)
10	9.87	9.71	8.38	8.42
12	9.89	9.73	8.35	8.47
14	9.79	9.57	8.34	8.46
16	9.80	9.79	8.34	8.48
18	9.80	9.79	8.46	8.48
20	9.81	9.76	8.47	8.48
22	9.82	9.76	8.47	8.48
24	9.82	8.73	8.46	8.47

stability and mechanical, electronic and structural properties of different SNTs and MSNTs with internal radii varying from 8 to 36 Å have been investigated in detail. The strain energy curves clearly show that the nanotubes are more energetically favorable compared to the respective sheet taken as reference. This is completely different from what is observed for other inorganic and carbon nanotubes. However, similar behavior has been previously observed by Seifert et al. [33] for the SiH nanotube using the same methodology. The results indicate that smaller radii are energetically favorable and probably converging to the amorphous system. However, it is important to highlight that the calculated structures are stable and can be seen as local minima in the potential energy surface which is obtained from the chrysotile nanotubes. The zigzag SNTs are about 0.5 meV.atom^{-1} more stable than the armchair SNTs due to the hydroxyl orientation. The chirality affects the MSNTs and the armchair is about 2 meV.atom^{-1} more stable than the zigzag MSNTs. This is probably due to the steric hindrance of the methyl groups in the zigzag structures. The strain energy of the MSNTs are about 2.5 meV.atom^{-1} more stable than the respective SNTs.

The SNT Young's moduli vary from 150 to 194 GPa and 232 to 360 GPa for zigzag and armchair chiralities, respectively. For the MSNTs the Young's moduli is in the range of 77–89 and 110–140 GPa for zigzag and armchair,

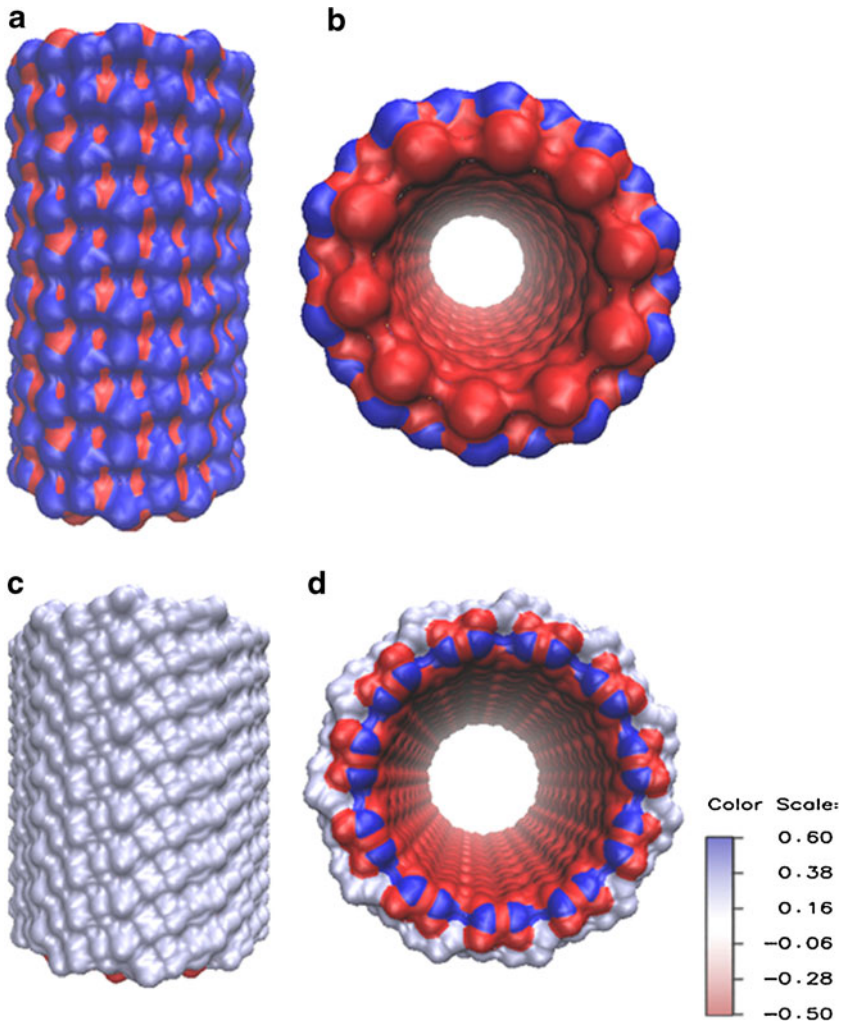

Fig. 9 Net electronic charge distribution of: SNT, surface view (**a**) and view along the tube's axis (**b**); MSNT surface view (**c**) and view along the tube's axis (**d**)

respectively. Furthermore, SNTs and MSNTs are insulators with band gaps around 9.8 and 8.5 eV, respectively. The modification of the outer surface of the SNTs with dimethyl silane groups lead to the decrease of the Young's moduli by about 100 GPa and the band gap by about 1 eV. The chrysotile nanotubes have band gaps of about 10 eV and Young's moduli in the range of 261 and 323 GPa estimated at the SCC-DFTB level of theory. These values must be compared to the silica and steel experimental values of 70 and 207 GPa, respectively. Finally the results show that silica *nano-fibriform* nanotubes are reasonably stable and their functionalization do not drastically modify the stability, electronic and mechanical properties and increase their external hydrophobicity.

Acknowledgments We would like to thank to Dr. Cláudio de Oliveira for the initial support of this work and for a copy of his computer program to build the tubular structures from the respective sheet. This work is supported by the Brazilian Initiative National Institute of Science and Technology for Mineral Resources, Water and Biodiversity – INCT-ACQUA (http://www.acqua-inct.org). The support from the Brazilian Agencies Conselho Nacional para o Desenvolvimento Científico e Tecnológico – CNPq and Fundação de Amparo a Pesquisa do Estado de Minas Gerais – FAPEMIG is gratefully acknowledged.

References

1. Iijima S (1991) Helical microtubules of graphitic carbon. Nature 354:56. doi:10.1038/354056a0
2. Tenne R, Margulis L, Genut M, Hodes G (1992) Polyhedral and cylindrical structures of tungsten disulfite. Nature 360:444–446. doi:10.1038/360444a0
3. Hernández E, Goze C, Bernier P, Rubio A (1999) Elastic properties of single-wall nanotubes. Appl Phys A 68:287–292. doi:10.1007/s003390050890
4. Hernández E, Goze C, Bernier P, Rubio A (1998) Elastic properties of C and $B_xC_yN_z$ composite nanotubes. Phys Rev Lett 80:4502–4505. doi:10.1103/PhysRevLett.80.4502
5. Köhler T, Frauenheim T, Hajnal Z, Seifert G (2004) Tubular structures of GaS. Phys Rev B 69:193403. doi:10.1103/PhysRevB.69.193403
6. Seifert G, Terrones H, Terrones M, Jungnickel G, Frauenheim T (2000) Structure and electronic properties of MoS_2 nanotubes. Phys Rev Lett 85:146–149. doi:10.1103/PhysRevLett.85.146
7. Guimarães L, Enyashin AN, Frenzel J, Heine T, Duarte HA, Seifert G (2007) Imogolite nanotubes: stability, electronic, and mechanical properties. ACS Nano 1:362–368. doi:10.1021/nn700184k
8. Guerra DL, Batista AC, Viana RR, Airoldi C (2010) Adsorption of methylene blue on raw and MTZ/imogolite hybrid surfaces: effect of concentration and calorimetric investigation. J Hazard Mater 183:81–86. doi:10.1016/j.jhazmat.2010.06.109
9. Guerra DL, Batista AC, Viana RR, Airoldi C (2011) Adsorption of rubidium on raw and MTZ- and MBI-imogolite hybrid surfaces: an evidence of the chelate effect. Desalination 275:107–117. doi:10.1016/j.desal.2011.02.029
10. Ju S, Lin K, Lin K (2012) Electronic and structural properties of ultrathin SiO_2 nanowires. J Phys Chem C 116:3918–3927. doi:10.1021/jp209436r
11. Liang Y, Xue B et al (2011) Preparation of silica nanowires using porous silicon as Si source. Appl Surf Sci 258:1470–1473. doi:10.1016/j.apsusc.2011.09.109
12. Yu DP, Hang QL et al (1998) Amorphous silica nanowires: Intensive blue light emitters. App Phys Lett 73:3076–3079. doi:10.1063/1.122677
13. Wang L, Lu A, Wang C, Zheng X, Zhao D, Liu R (2006) Nanofibriform production of silica from natural chrysotile. J Colloid Interf Sci 295:436–439. doi:10.1016/j.jcis.2005.08.055
14. Wang L, Lu A et al (2006) Porous properties of nano-fibriform silica from natural chrysotile. Acta Geol Sin-Enl 80:180–184. doi:10.1111/j.1755-6724.2006.tb00228.x
15. Wang L, Lu A, Xiao Z, Ma J, Li Y (2009) Modification of nanofibriform silica by dimethyldichlorosilane. Appl Surf Sci 255:7542–7546. doi:10.1016/j.apsusc.2009.04.024
16. Kim K, Park S (2012) Influence of 1-D silica nanotubes as drug adsorbent on release behaviors of tulobuterol-loaded porous microcapsules. Colloid Surf B 92:240–245. doi:10.1016/j.colsurfb.2011.11.048
17. Bai W, Yang YJ, Tao X, Chen JF, Tan TW (2012) Immobilization of lipase on aminopropyl-grafted mesoporous silica nanotubes for the resolution of (R, S)-1-phenylethanol. J Mol Catal B 76:82–88. doi:10.1016/j.molcatb.2011.11.005
18. Tang H, Liew K, Li J (2012) Cobalt catalysts supported on silica nanotubes for Fischer-Tropsch synthesis. Sci China Chem 55:145–150. doi:10.1007/s11426-011-4440-6
19. Lourenço MP, de Oliveira C, Oliveira AF, Guimarães L (2012) Structural, electronic, and mechanical properties of single-walled chrysotile nanotube models. J Phys Chem C 116:9405–9411. doi:10.1021/jp301048p
20. Oliveira AF, Seifert G, Heine T, Duarte HA (2009) Density-functional based tight-binding: an approximate DFT method. J Braz Chem Soc 20:1193–1205. doi:10.1590/S0103-50532009000700002
21. Elstner M, Porezag D et al (1998) Self-consistent-charge density-functional tight-binding method for simulations of complex materials properties. Phys Rev B 58:7260–7268. doi:10.1103/PhysRevB.58.7260
22. Frauenheim T, Seifert G et al (2002) Atomistic simulations of complex materials; ground-state and excited-state properties. J Phys Cond Matter 14:3015–3047. doi:10.1088/0953-8984/14/11/313
23. Density functional based Tight Binding (and more). http://www.dftb-plus.info/. Accessed 21 August 2012
24. Frenzel J, Oliveira AF, Duarte HA, Heine T, Seifert G (2005) Structural and electronic properties of bulk gibbsite and gibbsite surfaces. Z Anorg Allg Chem 631:1267–1271. doi:10.1002/zaac.200500051
25. Luschtinetz R, Oliveira AF et al (2008) Adsorption of phosphonic and ethylphosphonic acid on aluminum oxides surface. Surf Sci 602:1347–1359. doi:10.1016/j.susc.2008.01.035
26. Luschtinetz R, Frenzel J, Milek T, Seifert G (2009) Adsorption of phosphonic acid at the TiO_2 anatase (101) and rutile (110) surface. J Phys Chem C 113:5730–5740. doi:10.1021/jp8110343
27. dftb.org the DFTB website. http://www.dftb.org/parameters/. Accessed 21 August 2012
28. Nelder JA, Mead R (1965) A simplex method for function minimization. Comp J 7:308–314
29. Yarbro LA, Deming SN (1974) Selection and preprocessing of factors for simplex optimization. Anal Chim Acta 73:391–398. doi:10.1016/S0003-2670(01)85476-3
30. Press WH, Teukolsky SA, Vetterling WT, Flannery BP (1999) Numerical recipes in C: the art of scientific computing, 2nd edn. Cambridge University Press, Cambridge, pp 408–412
31. Monkhorst HJ, Pack JD (1976) Special points for Brillouin-zone integrations. Phys Rev B 13:5188–5192. doi:10.1103/PhysRevB.13.5188

32. Nicholas JB, Hopfinger AJ, Trouw FR, Iton LE (1991) Molecular modeling of zeolite structure. 2. Structure and dynamics of silica sodalite and silicate force field. J Am Chem Soc 113:4792–4800. doi:10.1021/ja00013a012
33. Seifert G, Köhler T, Urbassek HM, Hernández E, Frauenheim T (2001) Tubular structures of silicon. Phys Rev B 63:193409. doi:10.1103/PhysRevB.63.193409
34. Marana NL, Sambrano JR, de Souza AR (2010) Propriedades eletrônicas, estruturais e constantes elásticas do ZnO. Química Nova 33:810–815. doi:10.1590/S0100-40422010000400009
35. Oh ES (2010) Elastic properties of boron-nitride nanotubes through the continuum lattice approach. Mater Lett 64:859–862. doi:10.1016/j.matlet.2010.01.041
36. Lier GV, Alsenoy CV, Doren VV, Geerling P (2000) *Ab initio* study of the elastic properties of single-walled carbon nanotubes and graphene. Chem Phys Lett 326:181–185. doi:10.1016/S0009-2614(00)00764-8
37. Guimarães L, Enyashin AN, Seifert G, Duarte HA (2010) Structural, electronic, and mechanical properties of single-walled halloysite nanotube models. J Phys Chem C 114:11358–11363. doi:10.1021/jp100902e